Int. J. Heat Mass Transfer. Vol. 33, No. 5, pp. 943–952, 1990
Printed in Great Britain

0017-9310/90 $3.00 + 0.00

Convective heat transfer to laminar droplet flow in tube bundles

T. H. HWANG
Department of Mechanical Engineering, University of Hawaii at Manoa, Honolulu, HI 96822, U.S.A.

(*Received* 9 *March* 1989 *and in final form* 22 *August* 1989)

Abstract—Convective heat transfer of longitudinal laminar droplet flow in the thermal entrance region of tube bundles is analyzed for constant wall temperature and constant heat flux conditions, respectively. The tube bundle geometry is taken into consideration based on the free-surface model. The saturated droplets in the superheated vapor stream are considered as distributed heat sinks. Calculations are performed for the variations of droplet size, vapor velocity, droplet number density and the local Nusselt number in the streamwise direction until the single-phase fully-developed condition is reached. The effects of different governing parameters on the heat transfer results are studied.

1. INTRODUCTION

SPRAY COOLING heat transfer has received considerable attention because of its wide applications, such as in the metallurgical industry, nuclear safety analysis and cooling design of supercomputers. In particular, spray cooling has been recognized as one of the important emergency core cooling systems for Boiling Water Reactors during the loss-of-coolant accident. In the emergency spray cooling process, water droplets are injected into the superheated vapor stream in the bundle to cool the hot core and prevent the fuel rods from melt down before the reflood quench front arrives. The presence of saturated droplets in the superheated vapor stream augments the vapor heat transfer from the hot rod surface. In addition, the droplets evaporate and generate saturated vapor, therefore accelerating the vapor stream.

A general approach has been used to study droplet flow in tube bundles [1] by regarding the droplets as equivalent heat sinks distributed in the vapor stream. Sun *et al.* [1] studied the fully-developed laminar droplet flow heat transfer by assuming a uniform vapor velocity profile and a zero axial temperature gradient of the vapor. The tube bundle was treated as a system of parallel subchannels, where each channel represents a unit cell. The subchannel was then characterized by a circular pipe with the same hydraulic diameter. Their analysis was extended for the parabolic velocity profile by Dix and Anderson [2]. Wong and Hochreiter [3] further analyzed the heat transfer results for three different geometries with the same hydraulic diameter—an infinite square array of cylindrical rods, an annulus and a circular pipe. They concluded that the results for the equivalent annulus and the rod bundles agree well, and the circular pipe is in general a poor approximation for rod bundle geometries. Although the heat transfer characteristics of the fully-developed droplet flow are well understood, relatively little information is known for droplet flow in the thermal entrance region of the bundles.

The heat sink concept has been successfully adopted by Yao and Rane [4–6] for predicting the laminar droplet flow heat transfer in the thermal entrance region of a circular tube. The diminishing of droplet size, the increase of vapor velocity and the dilution of droplet number density along the tube were considered in their studies. The effects of dimensionless parameters such as the liquid loading, heat sink and wall superheated on the droplet flow heat transfer were also discussed. It was concluded that the classical laminar vapor flow heat transfer is a special case of the laminar droplet flow heat transfer phenomena.

In analyzing single-phase, longitudinal laminar flow in tube bundles, Happel [7] has developed a simple 'free-surface model' for predicting the complicated hydrodynamic behavior in different bundle geometries. This model reduces the complex problem of the multicylinder assemblage by considering an equivalent concentric cylindrical cell around a cylinder. The interaction of a particular cylinder with its neighbors is represented by this cylindrical cell. The hypothetical fluid cell is assumed to have zero shear stress at its outer surface. The fluid-to-cylinder volume ratio in the entire assemblage is preserved in this cell. The free-surface model was further extended by Hwang and Yao [8] for predicting the convective heat transfer to crossflow in tube bundles. Generally speaking, a detailed finite difference solution within a channel formed by adjacent tubes in a bundle is more reliable but more difficult since azimuthal variations in vapor velocity and temperature are introduced. Consequently, tremendous computing time is required for such a three-dimensional approach. On the other hand, because of the close resemblance in geometric configurations and boundary conditions, the free-surface model (or equivalent annulus approach) appears to be a good approximation for tube bundle geometry

NOMENCLATURE

A	liquid loading parameter, defined in equation (14)
C	wall superheat parameter, defined in equations (26) and (27)
C_p	specific heat of vapor
D	dimensionless droplet diameter, d/d_0
d	droplet diameter
d_0	droplet diameter at thermal entrance ($x = 0$)
h_d	heat transfer coefficient for evaporating droplets
h_{fg}	latent heat of evaporation
h_p	heat transfer coefficient of non-evaporating droplet or solid sphere with diameter of d, $2k/d$
h_{p0}	heat transfer coefficient of non-evaporating droplet or solid sphere with diameter of d_0, $2k/d_0$
k	thermal conductivity of vapor
n	droplet number density (number of droplets per unit volume)
n_0	droplet number density at thermal entrance
Nu_x	local Nusselt number, defined by equations (30) and (31)
Pr	Prandtl number of vapor, $\mu C_p/k$
P_h	horizontal pitch of tube bundles
P_v	vertical pitch of tube bundles
Q_w	dimensionless local heat flux at the wall, defined in equation (32)
q_w	heat flux at the wall
R	dimensionless radial position, r/r_0
R^*	dimensionless radius of unit cell, r^*/r_0
Re	Reynolds number for vapor, $2V_0r_0/\nu$
r	radial position
r_0	radius of tube
r^*	radius of unit cell
S	heat sink parameter, defined in equation (19)
T	temperature of vapor
T_m	bulk mean temperature of vapor
T_s	saturated temperature
T_w	wall temperature
V	mean vapor velocity
V_0	mean vapor velocity at thermal entrance
V_x	mean vapor velocity as droplets evaporate completely
V'	vapor velocity
x	axial position in thermal entrance region
X	dimensionless axial position, $(x/r_0)/(Re \cdot Pr)$
z_0	flow quality at thermal entrance.

Greek symbols

α_0	vapor void fraction at $x = 0$
β	ratio of the cell radius to the tube radius, r^*/r_0
γ	constant
ε	porosity of tube bundles, defined in equation (1c)
θ	dimensionless vapor temperature, defined in equations (16) and (17)
θ_m	dimensionless vapor bulk mean temperature
θ_w	dimensionless wall temperature
λ	parameter of tube bundles, defined in equation (3)
μ	dynamic viscosity of vapor
ν	kinematic viscosity of vapor
ρ_l	liquid density
ρ_v	vapor density.

when the pitch-to-tube diameter ratio is large [3, 7, 8].

The present analysis adopts the free-surface model [7] and Yao's heat sink approach [4–6] to study the convective heat transfer of longitudinal laminar droplet flow in the thermal entrance region of tube bundles.

2. MODEL AND FORMULATION

Figure 1 shows the typical staggered array and in-line array tube bundles with the droplet flow in the longitudinal direction, where P_h and P_v are the horizontal and vertical pitch in the bundles, respectively. With the use of the free-surface model, the hydrodynamics in tube bundles can be analyzed on a tube which has a radius r_0 surrounded by a cylindrical cell of fluid with a free surface at radius r^*, as shown in Fig. 2(a). The unit cell radius r^* in the free-surface model is related to bundle pitches P_h and P_v as

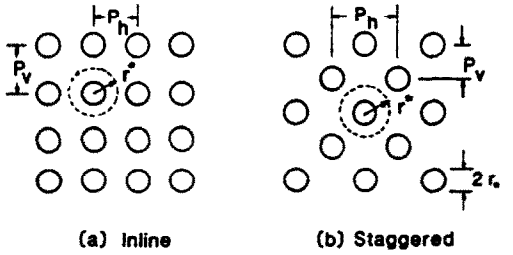

FIG. 1. Typical layout of tube bundles.

$$r^* = \left(\frac{P_h P_v}{\pi}\right)^{1/2}. \tag{1a}$$

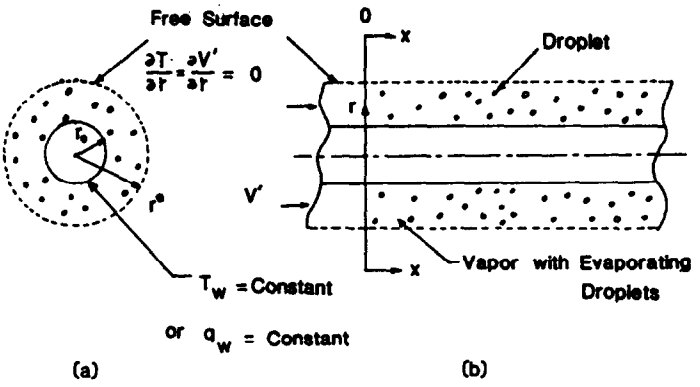

FIG. 2. Schematic of droplet flow heat transfer in the thermal entrance region of tube bundles.

The porosity of a tube bundle ε can also be related to the bundle pitches as

$$\varepsilon = \frac{P_h P_v - \pi r_0^2}{P_h P_v}. \tag{1b}$$

The ratio of the cell radius to the tube radius, β, can be related to the porosity ε of the bundle as

$$\beta = r^*/r_0 = \left(\frac{1}{1-\varepsilon}\right)^{1/2}. \tag{1c}$$

By neglecting the circumferential variation, the fully-developed vapor velocity distribution in the cylindrical unit cell can be approximated as

$$V' = \left\{\frac{\beta^2}{2}\ln\left(\frac{r}{r_0}\right) - \frac{1}{4}\left[\left(\frac{r}{r_0}\right)^2 - 1\right]\right\}\frac{V}{\lambda} \tag{2}$$

where V is the mean vapor velocity which will vary along the stream due to the vapor generation from droplets in the present study, and

$$\lambda = \left\{\frac{\beta^4 \ln \beta}{2(\beta^2-1)}\right\} - \tfrac{1}{8}\{3\beta^2 - 1\} \tag{3}$$

is a parameter of tube bundles in terms of bundle porosity ε. It is interesting to note that the velocity profile in equation (2) depends only on bundle porosity ε instead of the details of bundle geometry, because of the application of the free-surface model. It has been reported [7] that the free-surface is not applicable for a bundle porosity lower than 0.5, which corresponds to a pitch-to-tube diameter ratio of 1.25. For close-packing bundles, the interaction of the surrounding tubes on the hydrodynamic behavior of the flow becomes important and the circumferential variation of vapor velocity cannot be neglected. Modifications of equation (2) will be needed as the tube spacing becomes smaller. These restrictions of the free-surface model are also applicable to the present analysis.

In this paper, an analysis is performed for droplet flow in the thermal entrance region of tube bundles with the following assumptions.

(1) Fluid properties are constant and the vapor velocity profile is fully-developed.

(2) Flow quality is high ($z_0 > 0.5$) so that droplets travel at the same velocity as the vapor and the momentum of droplets has no influence on the vapor velocity profile.

(3) Droplet size is uniform at any tube bundle cross-section.

(4) Thermal radiation and droplet–wall contact heat transfer are neglected.

(5) Circumferential variation of vapor temperature is neglected.

It is known that the vapor velocity profiles are fully-developed at both the inlet of the thermal entrance region and its fully-developed condition of single-phase flow, where all the droplets evaporate completely. At the middle part of the thermal entrance region the vapor velocity may deviate from the fully-developed profile due to the strong evaporation of droplets near the hot wall. However, if the droplet number density is not very high, the fully-developed vapor flow may not be seriously affected by the non-uniform evaporation of droplets. As a first attempt to predict the heat transfer characteristics of laminar droplet flow in the thermal entrance region of tube bundles, a fully-developed velocity with mean vapor velocity varying along the bundle, due to the droplets' evaporation, is considered in this study. Furthermore, it is beyond the scope of the present work to investigate the detailed hydrodynamics of droplet flow in tube bundles. Hence, following refs. [1, 3–6], it was decided that detailed calculations using coupled mass, momentum and energy equations considering refined local velocity profiles will not be performed in the present study.

The schematic of droplet flow heat transfer in the cylindrical unit cell is shown in Fig. 2(b). The droplets in the vapor flow are regarded as heat sinks. Heat is transferred from the superheated vapor to the saturated droplet, and the subsequently generated vapor is heated up to the vapor stream temperature. With these heat sink considerations and the assumptions

described above, the energy equation for the vapor phase in a cylindrical unit cell can be formulated as

$$\rho_v C_p V' \frac{\partial T}{\partial x} = \frac{k}{r}\frac{\partial}{\partial r}\left(r\frac{\partial T}{\partial r}\right) - n\pi d^2 h_d \cdot \left\{1+\frac{C_p(T-T_s)}{h_{fg}}\right\}(T-T_s) \quad (4)$$

where the last term represents the heat sink contribution [6] with h_d denoting the heat transfer coefficient from superheated vapor to a saturated droplet, which is given [9, 10] by

$$h_d = \frac{h_p}{\{1+(C_p(T-T_s)/h_{fg})\}^{\gamma}} \quad (5)$$

where h_p is the heat transfer coefficient of an equivalent non-evaporating droplet or solid sphere and γ is in the range of 0.7–1.0. In this study, γ is selected as 1.0 for simplicity. For small size of droplet or sphere, h_p can be approximated as $2k/d$ [5, 11].

The initial and boundary conditions of equation (4) are

$$T = T_s \quad \text{at} \quad x = 0 \quad (6)$$

$$\frac{\partial T}{\partial r} = 0 \quad \text{at} \quad r = r^* \quad (7)$$

and

$$T = T_w \quad \text{at} \quad r = r_0 \quad (8)$$

for the constant wall temperature condition, or

$$-k\frac{\partial T}{\partial r} = q_w \quad \text{at} \quad r = r_0 \quad (9)$$

for the constant wall heat flux condition. Here, equation (7) is the boundary condition on the free surface of the cylindrical unit cell.

Note that droplet diameter in equation (4) is not constant due to evaporation along the stream. With the use of assumptions (2) and (3) and the energy balance on a droplet, this gives

$$\pi d^2 h_d (T_m - T_s) = -\tfrac{1}{2}\rho_l h_{fg}\pi d^2 V \frac{dd}{dx} \quad (10)$$

which is to be solved subject to the initial condition

$$d = d_0 \quad \text{at} \quad x = 0. \quad (11)$$

In equation (10) T_m is the local vapor bulk mean temperature, which is given by

$$T_m = \frac{2}{\lambda(\beta^2-1)r_0^2}\int_{r_0}^{r^*} T\left\{\frac{\beta^2}{2}\ln\left(\frac{r}{r_0}\right) - \frac{1}{4}\left[\left(\frac{r}{r_0}\right)^2 - 1\right]\right\} r\,dr. \quad (12)$$

The droplet size can also be presented in terms of droplet number density by the mass balance on the droplets, which gives

$$\frac{n_0}{n} = 1 + A\left\{1-\left(\frac{d}{d_0}\right)^3\right\} = \frac{V}{V_0} \quad (13)$$

where

$$A = \frac{n_0\pi d_0^3}{6}\left(\frac{\rho_l}{\rho_v}\right) = (1-\alpha_0)\cdot\frac{\rho_l}{\rho_v} \quad (14)$$

is the liquid loading parameter, n_0 is the droplet number density and α_0 the vapor void fraction evaluated at $x = 0$. A numerical solution of equation (4), together with equations (10) and (13), gives the variations of mean vapor velocity and droplet number density along the tube length.

We now introduce the following dimensionless quantities:

$$R = r/r_0, \quad D = d/d_0, \quad X = \left(\frac{x}{r_0}\right)\Big/(Re\cdot Pr) \quad (15)$$

and

$$\theta = \frac{T-T_s}{T_w-T_s} \quad (16)$$

for the constant wall temperature condition, or

$$\theta = \frac{k(T-T_s)}{q_w r_0} \quad (17)$$

for the constant wall heat flux condition, where $Re = 2\rho_v V_0 r_0/\mu$ and $Pr = \mu C_p/k$. Substituting equations (2) and (3) into equation (4) the resulting energy equation for vapor in dimensionless form is

$$\frac{1}{2\lambda}\left\{\frac{\beta^2}{2}\ln R - \tfrac{1}{4}(R^2-1)\right\}\{1+A(1-D^3)\}\frac{\partial\theta}{\partial X} = \frac{1}{R}\frac{\partial}{\partial R}\left(R\frac{\partial\theta}{\partial R}\right) - \left\{\frac{D\cdot S}{1+A(1-D^3)}\right\}\theta \quad (18)$$

where

$$S = n_0\pi d_0^2 h_{p0} r_0^2/k = 6A\cdot\left(\frac{h_{p0}d_0}{k}\right)\left(\frac{r_0^2}{d_0^2}\right)\left(\frac{\rho_v}{\rho_l}\right) \quad (19)$$

is the heat sink parameter. Equation (18) is to be solved with the initial and boundary conditions

$$\theta = 0 \quad \text{at} \quad X = 0 \quad (20)$$

$$\frac{\partial\theta}{\partial R} = 0 \quad \text{at} \quad R = R^* = \beta \quad (21)$$

and

$$\theta = 1 (T_w = \text{constant}) \quad \text{at} \quad R = 1 \quad (22)$$

or

$$\frac{\partial\theta}{\partial R} = 1 (q_w = \text{constant}) \quad \text{at} \quad R = 1. \quad (23)$$

The dimensionless droplet diameter D in equation (18) can be determined from equation (10) together with equation (5)

$$D\{1+A(1-D^3)\}\frac{dD}{dX} = -\frac{2}{3}\left(\frac{\theta_m}{C^{-1}+\theta_m}\right)\frac{S}{A} \quad (24)$$

which is to be solved with the initial condition

$$D = 1 \quad \text{at} \quad X = 0 \tag{25}$$

where C is the wall superheat parameter which is given by

$$C = \frac{C_p}{h_{fg}}(T_w - T_s) \tag{26}$$

for the constant wall temperature condition, or

$$C = \frac{C_p q_w r_0}{k h_{fg}} \tag{27}$$

for the constant heat flux condition. After θ is solved from equation (18), the bulk mean temperature of vapor can be calculated from

$$\theta_m = \frac{2}{\lambda(\beta^2 - 1)} \int_1^{R^*} \theta \left\{ \frac{\beta^2}{2} \ln R - \tfrac{1}{4}(R^2 - 1) \right\} R \, dR. \tag{28}$$

Equations (18)–(25) with four parameters A, S, C and ε are the governing equations for drolet flow in the thermal entrance region of the tube bundles. These equations were solved numerically based on the finite difference method. Calculations for the variations of droplet size, vapor velocity and local Nusselt number were carried out in the streamwise direction until the thermal fully-developed condition is reached. The axial increment of X is set to 0.0001. The radial increment of R is selected as 0.0173, 0.03 and 0.044 for tube bundles with a porosity of 0.65, 0.91 and 0.95, respectively. Numerical results have been obtained for the liquid loading parameter A varying from 0.2 to 1.0, the heat sink parameter S varying from 0 to 200, and the wall superheat parameter C ranging from 0.1 to 10.0 with the constant wall temperature or constant wall heat flux condition. The present results of Nusselt number for single-phase flow (i.e. $S = 0$) at the thermal fully-developed condition are found to be in satisfactory agreement with the solutions presented in refs. [12–15].

3. RESULTS AND DISCUSSION

As discussed in the preceding section, there exists three dimensionless droplet flow parameters A, S and C, as well as one dimensionless tube bundle porosity ε in the present analysis. The liquid loading parameter A characterizes the amount of liquid droplets in the vapor. The heat sink parameter S characterizes the degree of liquid droplet dispersion in the vapor flow. The wall superheat parameter C characterizes the degree of wall superheat and the bundle porosity ε characterizes the vapor flow field in the bundle. It can be seen further from equation (19) that for a given liquid loading A, the value of S is inversely proportional to the surface area of a droplet. Therefore, a large value of S means a strong heat sink effect, a small droplet size and a large droplet number density at the thermal entrance. It also implies fast droplet evaporation and gives a high heat transfer rate from the wall.

Figure 3 represents the variation of vapor velocity with the axial location. The vapor velocity increases along the tube because of the evaporation of droplets. The stronger the heat sink effect the faster the droplets evaporate, and therefore the vapor velocity increases faster along the tube. Eventually, all the droplets are evaporated and the flow becomes single-phase vapor flow. The final vapor velocity V_∞ depends on the initial liquid loading parameter A as indicated in equation (13) and Fig. 3. Furthermore, using the homogeneous flow model [16], the final vapor velocity can be expressed as

$$V_\infty = (1 + A) \cdot V_0 \approx \frac{V_0}{z_0} \tag{29}$$

where the initial liquid loading parameter A is approximated by $(1 - z_0)/z_0$ with z_0 denoting the flow quality at the thermal entrance.

Figures 4(a) and (b) depict the variation of local Nusselt number of droplet flow with the axial location for tube bundles with a porosity of 0.65 at the constant wall temperature and constant heat flux conditions, respectively. The heat sink parameters are set to 60 and 200 with the liquid loading parameter varying from 0.2, 0.6 to 1.0. The local Nusselt number of droplet flow is defined as

$$Nu_x = \frac{2 q_w r_0}{k(T_w - T_m)} = \frac{2}{\theta_m - 1} \cdot \left. \frac{\partial \theta}{\partial R} \right|_{R=1} \tag{30}$$

for the constant wall temperature condition, or

$$Nu_x = \frac{2 q_w r_0}{k(T_w - T_m)} = \frac{2}{\theta_w - \theta_m} \tag{31}$$

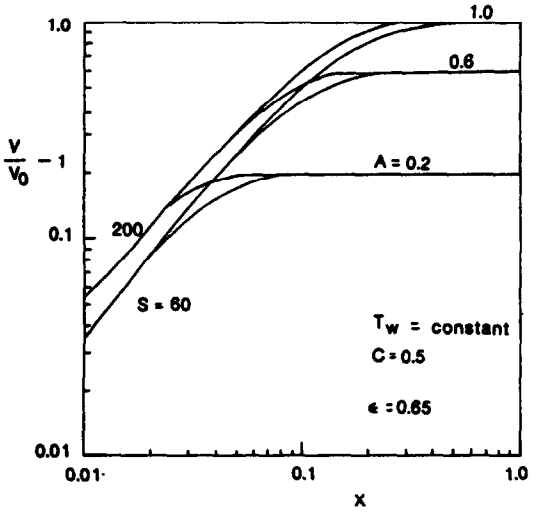

FIG. 3. The variation of mean vapor velocity with axial location for the constant wall temperature condition.

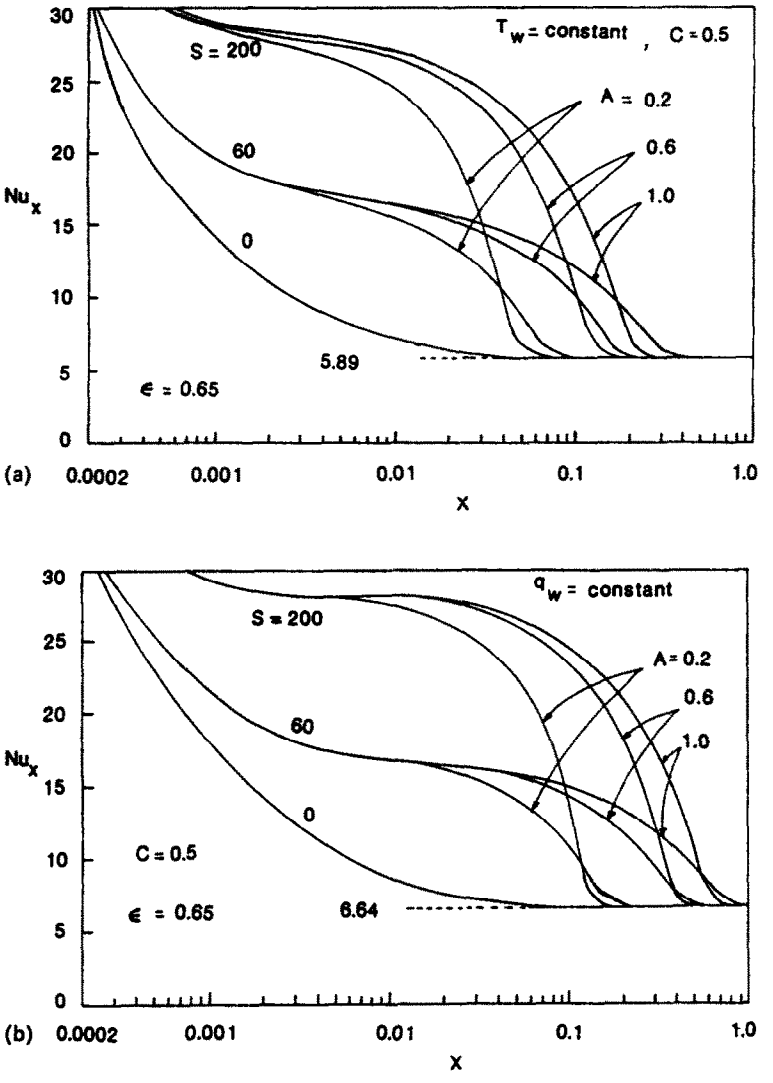

FIG. 4. The variation of local Nusselt number with axial location at (a) constant wall temperature and (b) constant heat flux.

for the constant heat flux condition. Figures 4(a) and (b) show that the local Nusselt number increases with the values of S and A, which demonstrates the significant heat transfer effect of droplets in the vapor flow. For the limiting case of $S = 0$ (which means single-phase vapor flow) the present results of the Nusselt number for thermal fully-developed flow are in good agreement with those presented in refs. [12–15].

It is noted that equation (19) indicates that for a given value of S, a large value of A implies the droplet size is large at the thermal entrance; therefore, as indicated in Fig. 4, such a droplet flow travels far before all the droplets are evaporated completely. On the other hand, for a given value of A, a large value of S means that the droplet size is small at the thermal entrance and consequently the droplets evaporate early. Figure 4 shows that for a small value of S, say $S = 60$, the effect of liquid loading A on heat transfer is not significant at the beginning of the thermal entrance region. This could be attributed to the low heat sink effect, that the droplets evaporate slowly at the beginning of the thermal entrance, and that the size of droplets, in terms of the liquid loading A, is not influential to heat transfer from the wall. As the droplet size gets smaller along the tube, the surface-to-volume ratio of a droplet increases sharply. Consequently, the liquid loading effect on the local Nusselt number becomes profound.

A comparison of Figs. 4(a) and (b) indicates a similar trend of variation for the local Nusselt number with axial location for the constant wall temperature condition and the constant wall heat flux condition. However, the Nusselt number of the constant heat flux case is higher than that of the constant temperature case with the same inlet condition.

The variation of the dimensionless mean vapor temperature θ_m is shown in Fig. 5(a) for the constant wall

temperature case, and in Fig. 5(b) for the constant heat flux case. For a given liquid loading A, a small value of heat sink parameter S means a small number of large droplets and less cooling of the vapor, which results in high mean vapor temperature along the tube, as indicated in Fig. 5. Eventually, all the droplets evaporate completely far downstream in all the cases. For the constant wall temperature condition, the mean vapor temperature approaches the wall temperature asymptotically. However, in the constant heat flux condition the mean vapor temperature increases linearly along the tube after the droplets have evaporated completely.

It is of interest to examine the variation of wall temperature along the tube for the constant heat flux condition. Figure 6 indicates that the larger the value of S, the higher the heat transfer rate and the slower the wall temperature increases. After all the droplets evaporate completely, the wall temperature increases linearly with the axial location as is well known in single-phase flow.

The variation of dimensionless droplet diameter D in the thermal entrance region is shown in Fig. 7 for the constant heat flux condition. Generally, the reduced rate of droplet size is faster as the droplet becomes smaller (say $D < 0.8$). As observed before, for a given liquid loading parameter A, the smaller the S the larger the droplet size, and the droplets travel a longer distance before they evaporate completely.

The effect of the wall superheat parameter C on the local Nusselt number Nu_x is shown in Fig. 8. The solid curves are for constant wall temperature and the dashed curves are for constant heat flux. It can be seen that the higher the wall superheat, the faster the droplets evaporate and the lower the local heat transfer along the tube. Hence the effect of the wall superheat parameter C is similar to that of the liquid loading parameter A but in the reverse trend.

Finally, the effect of tube bundle porosity ε on the heat transfer results is examined for the bundles with porosities of 0.91 and 0.95. Generally, the same trend of variations as that of $\varepsilon = 0.65$ is observed. However, the local Nusselt number for the bundle with the smallest tube spacing is higher than the other two at the same inlet condition. For a bundle with a large value of tube bundle pitch (i.e. a high value of ε), the vapor velocity gradient near the tube wall is small, which results in a low heat transfer rate. For a given

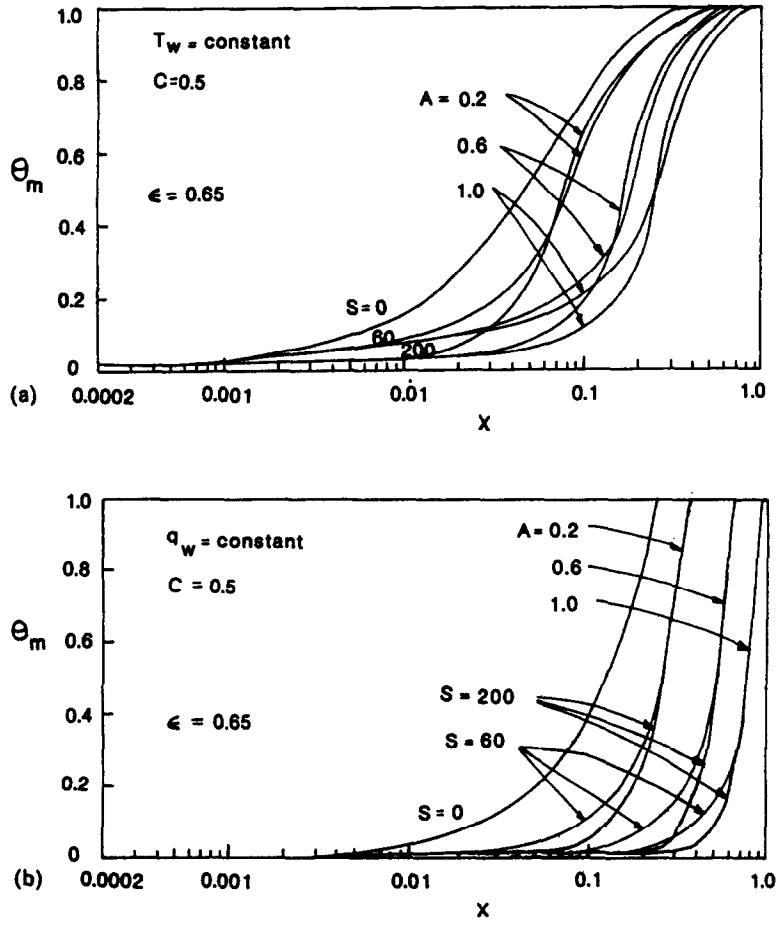

FIG. 5. The variation of mean vapor temperature with axial location at (a) constant wall temperature and (b) constant heat flux.

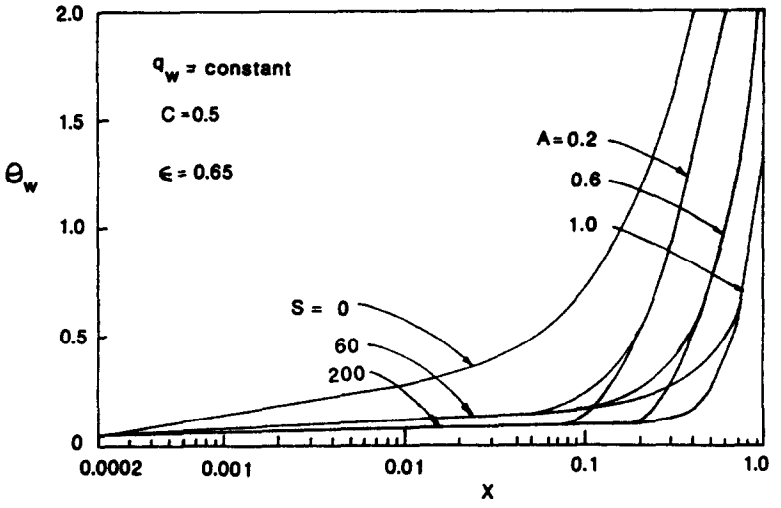

FIG. 6. The variation of wall temperature with axial location for the constant heat flux condition.

set of parameters A, S and C, the droplet size d_0 and the droplet number density n_0 at the thermal entrance are fixed. However, a high value of ε implies a large number of droplets, a small vapor velocity gradient near the wall and a low heat transfer rate. Thus, the droplets tend to travel far downstream before they evaporate completely. Another way to examine the effect of tube bundle porosity ε is to compare the local heat flux at the wall for various bundle geometries with the constant wall temperature condition. A non-dimensional local heat flux can be defined as

$$Q_w = \frac{2q_w r_0}{k(T_w - T_s)} = (1-\theta_m) \cdot Nu_x. \quad (32)$$

Figure 9 shows the variation of dimensionless local heat flux with the axial location for tube bundles with porosities of 0.65, 0.91 and 0.95 with a given set of governing parameters. The local heat flux for a higher heat sink parameter S, say $S = 100$, for a bundle with a porosity of 0.65 is also presented in Fig. 9 for comparison. As expected, at the same inlet condition the smaller the ε the higher the heat flux. It should be noted that, due to the application of the free-surface model, the details of bundle geometry (e.g. staggered or in-line array) have no effect on heat transfer results. Instead, tube bundle porosity ε has a significant effect on heat transfer results.

A comparison of the present results with experimental data was not possible due to the unavailability of such data. Further effort is needed to establish correlations of the four controlling parameters, A, S, C and ε, for predicting the heat transfer behavior of droplet flow in the thermal entrance region of tube bundles.

4. CONCLUSIONS

The laminar droplet flow heat transfer in the thermal entrance region of tube bundles has been investigated using the free-surface model and the heat sink

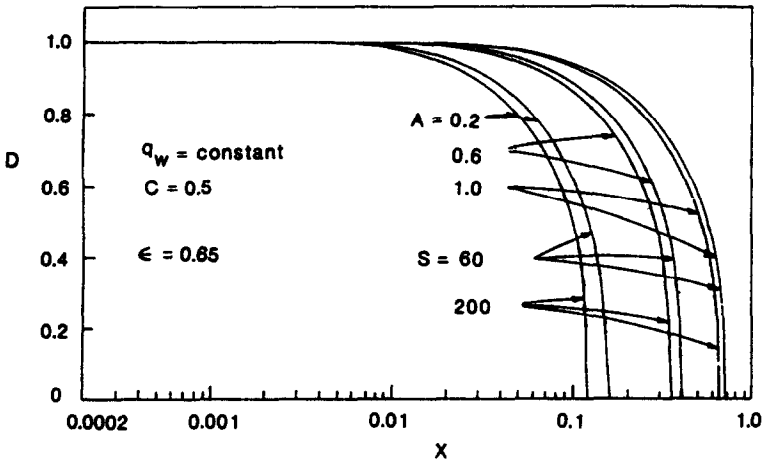

FIG. 7. The variation of droplet diameter with axial location for the constant heat flux condition.

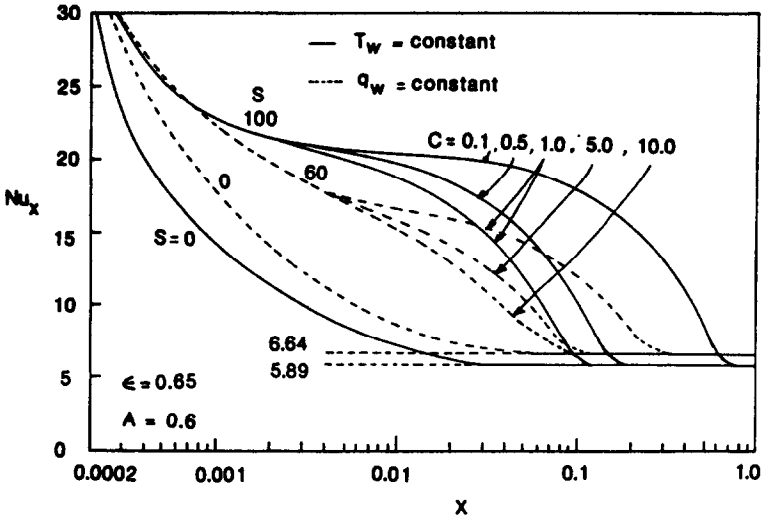

FIG. 8. The variation of local Nusselt number with wall superheat parameter C.

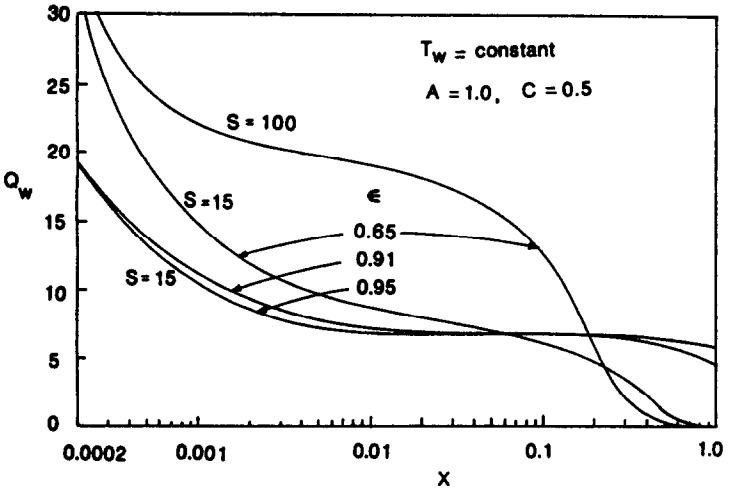

FIG. 9. The variation of local heat flux with axial location for various bundles using the constant wall temperature condition.

concept. The droplet size variation, vapor acceleration and dilution of droplet number density along the tubes have been considered. The effects of four governing parameters, namely the liquid loading parameter A, the heat sink parameter S, the wall superheat parameter C and the bundle porosity ε, on the heat transfer behavior of droplet flow are revealed.

Acknowledgements—I am grateful to the University of Hawaii Research Council for their financial support of this research project. I would also like to thank Professor P. Cheng at the University of Hawaii for his helpful suggestions and comments.

REFERENCES

1. K. H. Sun, J. M. Gonzalez-Santalo and C. L. Tien, Calculations of combined radiation and convective heat transfer in rod bundles under emergency cooling conditions, *J. Heat Transfer* **98**, 414–420 (1976).
2. G. E. Dix and J. G. M. Anderson, Spray cooling heat transfer for a BWR fuel rod bundle. In *Thermal and Hydraulic Aspects of Nuclear Reactor Safety* (Edited by O. C. Jones and S. G. Bankoff), Vol. 1, pp. 217–248. ASME, New York (1977).
3. S. Wong and L. E. Hochreiter, An analysis of heat transfer to axial dispersed flow between rod bundles under reactor emergency cooling conditions, *J. Heat Transfer* **102**, 508–512 (1980).
4. S. C. Yao, Convective heat transfer of laminar droplet flow in thermal entrance region of circular tubes, *J. Heat Transfer* **101**, 480–483 (1979).
5. S. C. Yao and A. Rane, Heat transfer of laminar mist flow in tubes, *J. Heat Transfer* **102**, 678–683 (1980).
6. A. Rane and S. C. Yao, Heat transfer of evaporating droplet flow in low pressure systems, *Can. J. Chem. Engng* **58**, 303–308 (1980).

7. J. Happel, Viscous flow relative to arrays of cylinders, *A.I.Ch.E. Jl* **5**, 174–177 (1959).
8. T. H. Hwang and S. C. Yao, Crossflow heat transfer in tube bundles at low Reynolds numbers, *J. Heat Transfer* **108**, 697–700 (1986).
9. M. Renksizbulut and M. C. Yuen, Experimental study of droplet evaporation in a high-temperature air stream, *J. Heat Transfer* **105**, 384–388 (1983).
10. M. C. Yuen and L. W. Chen, Heat transfer measurements for evaporating liquid droplets, *Int. J. Heat Mass Transfer* **21**, 537–542 (1978).
11. W. Ranz and W. Marshall, Jr., Evaporation from drops, *Chem. Engng Prog.* **48**, 141–146, 173–180 (1952).
12. E. M. Sparrow, A. L. Loffler, Jr. and H. A. Hubbard, Heat transfer to longitudinal laminar flow between cylinders, *J. Heat Transfer* **83**, 415–422 (1961).
13. A. J. Friedland and C. F. Bonilla, Analytical study of heat transfer rates for parallel flow of liquid metals through tube bundles, *A.I.Ch.E. Jl* **7**, 107–122 (1961).
14. O. E. Dwyer and H. C. Berry, Laminar-flow heat transfer for in-line flow through unbaffled rod bundles, *Nucl. Sci. Des.* **42**, 81–88 (1970).
15. J. H. Kim, Heat transfer in longitudinal laminar flow along circular cylinders in square array. In *Fluid Flow and Heat Transfer Over Rod or Tube Bundles* (Edited by S. C. Yao and P. A. Pfund), pp. 155–161. ASME, New York (1979).
16. J. G. Collier, *Convective Boiling and Condensation*. McGraw-Hill, New York (1981).

CONVECTION THERMIQUE POUR UN ECOULEMENT LAMINAIRE DE GOUTTELETTES DANS DES GRAPPES DE TUBES

Résumé—On analyse le transfert thermique pour un écoulement laminaire et longitudinal de gouttelettes dans la région d'entrée d'une grappe de tubes avec des conditions de température pariétale uniforme ou de flux pariétal uniforme. La géométrie de la grappe est prise en considération dans un modèle de surface libre. Les gouttelettes saturées, dans la vapeur surchauffée, sont considérées comme des puits de chaleur distribués. On fait des calculs pour différentes tailles de gouttes, vitesses de vapeur, populations de gouttes et on obtient le nombre de Nusselt local le long de l'écoulement jusqu'à la condition d'écoulement établi en monophasique. On étudie les effets sur le transfert thermique des différents paramètres qui interviennent.

KONVEKTIVER WÄRMEÜBERGANG BEI LAMINARER STRÖMUNG IN ROHRBÜNDELN

Zusammenfassung—Es wird der konvektive Wärmeübergang in einer längsgerichteten laminaren tropfenbeladenen Strömung im thermischen Einlaufgebiet eines Rohrbündels untersucht, und zwar für konstante Wandtemperatur und konstante Wärmestromdichte. Die Geometrie des Rohrbündels wird mit Hilfe eines Modells der freien Oberfläche berücksichtigt. Die gesättigten Tropfen in der überhitzten Dampfströmung werden als verteilte Wärmesenken betrachtet. Die Veränderungen der Tropfengröße, der Dampfgeschwindigkeit, der Tropfendichte und der örtlichen Nusselt-Zahl werden berechnet bis hin zum Zustand der einphasigen, vollständig entwickelten Strömung. Abschließend wird der Einfluß der unterschiedlichen Parameter auf den Wärmeübergang untersucht.

КОНВЕКТИВНЫЙ ТЕПЛОПЕРЕНОС ПРИ ЛАМИНАРНОМ КАПЕЛЬНОМ ТЕЧЕНИИ В ПУЧКАХ ТРУБ

Аннотация—Анализируется конвективный теплоперенос в начальном участке при продольном ламинарном капельном течении в пучке труб соответственно для условий постоянной температуры стенки и постоянного теплового потока. Геометрия пучка труб учитывается на основе модели свободной поверхности. Насыщенные капли в потоке перегретого пара рассматриваются как распределенные поглотители тепла. Выполнены расчеты, учитывающие изменение размера капель, скорости пра, плотности капель и локального числа Нуссельта до достижения полностью установившегося однофазного режима течения. Изучается влияние различных определяющих параметров на теплоперенос.